Annals of Nuclear Energy 127 (2019) 419–432 - DOI: 10.1016/j.anucene.2018.12.034

Uncertainty Quantification method for RELAP5-3D© using RAVEN and application on NACIE experiments

Vincenzo Narcisi*, Pierdomenico Lorusso*, Fabio Giannetti*, Andrea Alfonsi°, Gianfranco Caruso*

***DIAEE – Nuclear Section, "Sapienza" University of Rome, Corso Vittorio Emanuele II, 244, 00186, Rome, Italy**
°Idaho National Laboratory, Idaho Falls, Idaho, 83415

Keywords

- Gas-enhanced circulation
- Natural Circulation
- Heavy Liquid Metals (HML)
- Safety analysis
- Validation
- Thermal Hydraulics

Abstract

The best estimate plus uncertainty (BEPU) method plays a key role in the development of the innovative Generation IV nuclear reactors, for the improvement of knowledge and the good evaluation of the safety margins for new phenomena. The aim of this paper is to validate an uncertainty quantification (UQ) approach using RAVEN code. RAVEN, developed at the Idaho National Laboratory, is a multipurpose probabilistic and uncertainty quantification framework, capable to communicate with any system code, implemented with an integrated validation methodology involving several different metrics. In this activity, a coupled calculation RELAP5-3D/RAVEN has been performed to assess the validity of the embedded UQ approach. The simulations have concerned two tests conducted on NACIE (NAtural CIrculation Experiment) facility, a non-nuclear loop-type system using Lead-Bismuth Eutectic (LBE) as coolant, realized at the ENEA Brasimone Research Centre (Italy) to support the development of the GEN-IV reactors. The experimental tests are aimed to investigate the phenomena related to the natural and gas enhanced circulation flow regimes of heavy liquid metals (HLM), and to test and validate the main components in a LBE environment. A numerical 1D model of NACIE facility has been realized and the post-test analysis has been carried out using RELAP5-3D© ver. 4.3.4. Based on these results, a statistical analysis has been performed using RAVEN computer code, investigating the capability of three probabilistic comparison metrics fully integrated in the code.

1. Introduction

In recent years and in near future, nuclear energy is expected to play an important role in the frame of energy needs in terms of sustainability, safety, proliferation resistance and economy. Many

countries look with a rising interest in nuclear energy for electricity generation and non-electrical purposes. In this scenario, the GEN-IV systems, promoted by GIF (Generation IV International Forum) will increase the future growth and benefits deriving from nuclear energy utilization. The LFR (Lead-cooled Fast Reactors) is considered one of the most promising technologies to meet all the requirements introduced for GEN-IV reactors of sustainability, economics, proliferation resistance, safety and reliability. Several activities, under deployment in these years, aim to study the behaviour of molten lead-cooled systems in order to increase the knowledge and the experience performed in terms of design, operations, maintenance and materials for components.

The safety analysis plays a crucial role in the realization of these innovative nuclear power plant (NPP). In the past, the approach was to consider conservative assumption and boundary conditions to evaluate the safety margins of the NPP design. Different approach has been selected in the last applications (D'Auria et al., 2012, Queral et al., 2015): the best estimate calculation with uncertainty quantification.

The best estimate computer code, like RELAP5, was developed to investigate the behaviour of light water reactor (LWR) during postulated accidents (The RELAP5-3D© Code Development Team, 2015) and then improved in order to accomplish the safety analysis of the innovative reactors. In this framework, several R&D activities are funded to validate the improvement on the best estimate computer code and to develop methodologies for the quantification of the uncertainties.

The aim of this work is to verify the applicability of an uncertainty quantification-based methodology, and the analysis of the response through the use of different validation metrics. A set of N independent parameters are random sampled and introduced as input of M calculations, generating a set of M results. After a sufficiently large number of simulations, a statistical analysis is carried out obtaining information about the propagation of the input uncertainties to the output responses.

For this purpose, the LBE loop facility, called NACIE (NAtural CIrculation Experiment), has been modelled using RELAP5-3D© (R5-3D) and a statistical analysis was performed with a RELAP5-3D/RAVEN coupled calculation. The results have been compared with the experimental data to evaluate the merit of the methodology.

2. NACIE Facility

NACIE is a loop-type facility (Tarantino et al., 2010) cooled by LBE, designed and realized in the ENEA Brasimone Research Centre for the characterization of components, procedure and systems related to the HLM (Heavy Liquid Metals) nuclear technologies. The facility mainly consists of a primary LBE loop with a rectangular geometry, composed of two vertical pipes 7.5 m long, working as riser and downcomer respectively, connected by two horizontal pipes of 1 m, and a secondary water loop acting as heat sink. A schematic layout is reported in Fig. 1, while the main dimensions are summarized in Table 1.

The main components of the system are:

- the Fuel Pin Simulator (FPS), shown in Fig. 2, installed in the lower part of the riser and electrically heated for the coolant heating; it consists of two dummy pins to support the bundle itself and two electrical pins which can supply a total power of about 45 kW. The active length of the electrical pins is 850 mm and in the middle section of the active length

a spacer grid is located to allow the thermal expansion of the pins, keeping constant the flow area of the sub channel;

- the "tube in tube" Heat Exchanger (HX), located in the top part of the downcomer, operating in counter-flow regime and designed for a thermal duty of 30 kW. It essentially consists of three coaxial pipes: the inner pipe, in which the LBE flows, the middle pipe, forming with the inner one an annulus filled with AISI-304 stainless steel powder, and an outer pipe, which forms with the middle pipe an annulus region (the shell side) in which the water flows in counter-flow at low pressure (about 1.5 bar). The main view and characteristics of the HX are reported in Fig. 3 and Table 3, respectively;

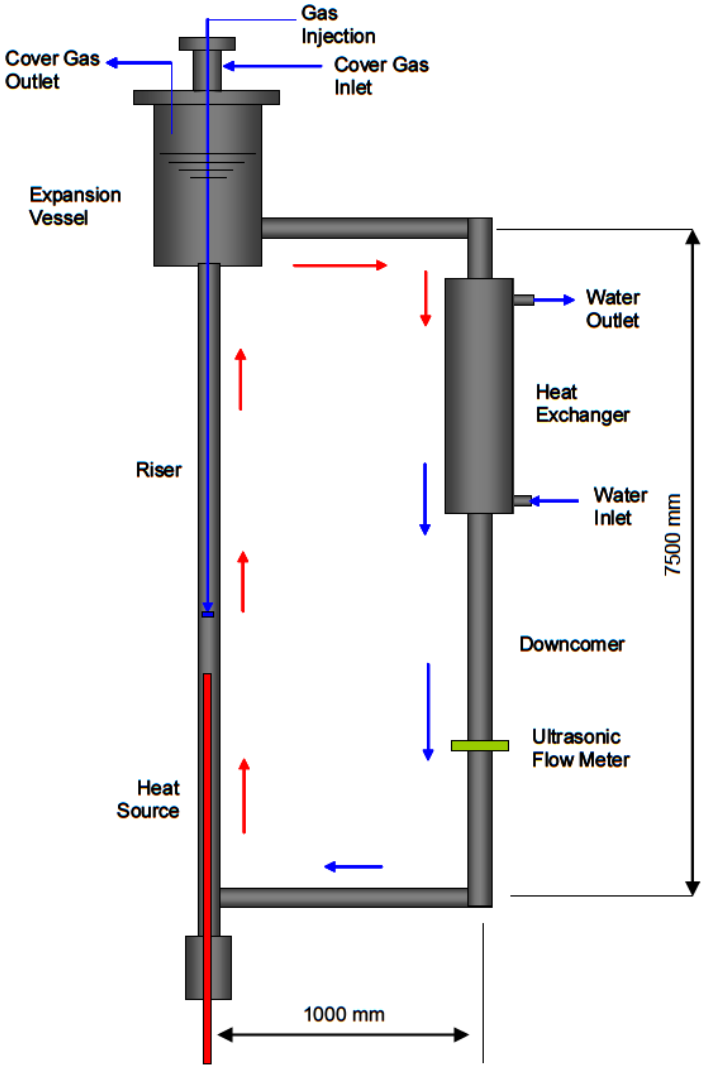

Fig. 1. Schematic layout of the system

- the gas injection device, inserted from the coupling flange in the upper part of the expansion tank, with the gas injector located in the middle of the riser, in order to enhance the liquid metal circulation. The gas injection system has been designed for an argon flow rate in the range 1-75 Nl/min with a maximum injection pressure of 5.5 bar;

- the expansion tank, located on the top of the riser which allows the separation between the phases (gas and LBE) in order to have the two-phase mixture in the riser only, between the gas injector and the exit nozzle in the expansion vessel;
- the pump, installed on the secondary loop to supply the requested water mass flow rate, and a fan cooler, used as final heat sink to guarantee the sub-cooling of the water.

All the pipes are in stainless steel AISI-304 with a nominal pipe diameter of 2 ½". The loop can contain an inventory of LBE of about 1000 kg and it allows a work internal pressure of 10 bar and a temperature of about 823 K.

The purpose of the AISI-304 powder is to guarantee the thermal flux towards water, since it has a good thermal conductivity, mitigating at the same time the thermal stresses on the pipes due to the differential axial thermal expansion.

Table 1. Main characteristic of NACIE loop (Shin et al., 2014)

Main dimensions of the loop	
Vertical Length [mm]	9231
Horizontal Length [mm]	1000
Pipe Inner Diameter [mm]	62.7
Pipe Thickness [mm]	5.16
Expansion Tank Height [mm]	765
Expansion Tank Inner Diameter [mm]	254.5
Heat Exchanger Height [mm]	1500

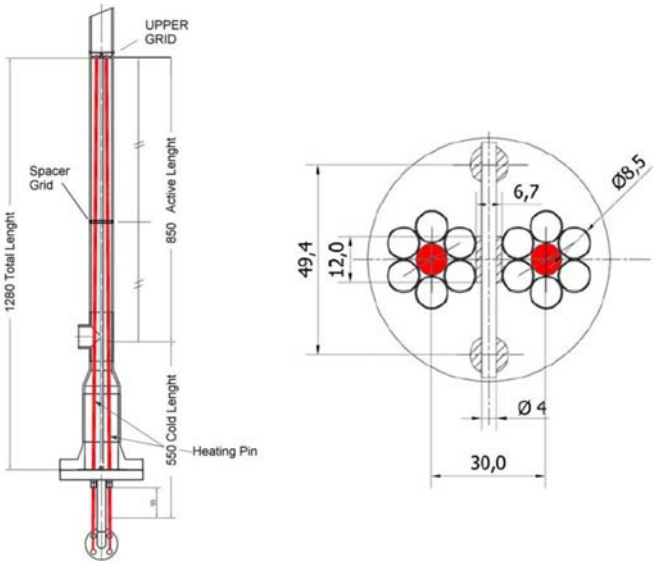

Fig. 2. General view (left) and section (right) of the NACIE bundle

Table 2. Main parameters of the FPS

Main characteristics of the FPS	
Number of active pins	2
Pin Diameter (mm)	8.2
Total length (mm)	850

Active length (mm)	1400
Heat Flux (W/cm^2)	100
Flux Distribution	Uniform
Thermal Power [kW]	22

Table 3. Main dimensions of the heat exchanger (Coccoluto et al., 2011)

Main dimensions of the HX

Parameters	Internal Pipe	Middle Pipe	External Pipe
Inner Diameter (mm)	62.68	84.9	102.3
Outer Diameter (mm)	73	88.9	114.3
Thickness (mm)	5.16	2	6.02
Length (mm)	1500	1500	1500
Material	AISI 304	AISI 304	AISI 304

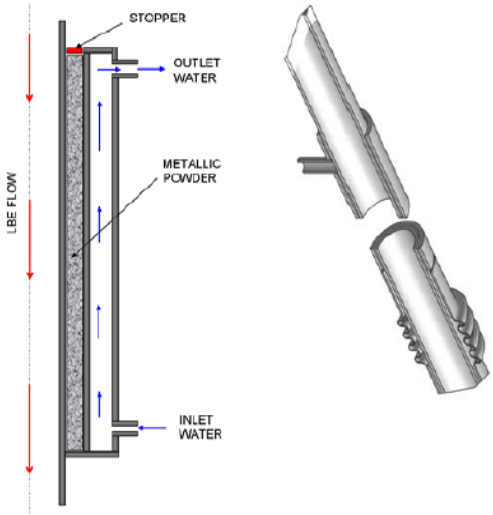

Fig. 3. View of the heat exchanger

3. RELAP5-3D model

The thermal-hydraulic behaviour of NACIE loop has been simulated by RELAP5-3D© ver. 4.3.4 thermal-hydraulic system code, using the most recent LBE thermo-physical properties correlations, recommended by NEA (OECD/NEA Nuclear Science Commitee, 2015) and implemented in R5-3D (Balestra et al., 2016). A 1D model of the loop has been constructed to gather information about the behaviour of the system for both natural and gas-enhanced flow regimes. A view of the primary loop nodalization is shown in Fig. 4. It is composed of 170 hydrodynamic volumes, 169 junctions, 174 heat structures and 3690 heat transfer nodes which reproduce the following components:

- the Fuel Pin Simulator: reproduced by PIPE 101;
- the Heat Exchanger: composed of PIPE 113 (LBE side) and PIPE 203 (shell side, water in counter-flow);
- the expansion vessel: composed of PIPE 107 and PIPE 109;
- the two vertical legs (PIPE 103, 105, 115, BRANCH 104) and the two horizontal legs (PIPE 111 and 117).

The argon injection device is reproduced by the time dependent volume (TMDPVOL) 301 which sets the gas inlet pressure and temperature, and the time dependent junction (TMDPJUN) 302 that imposes the gas inlet flow rate.

The TMDPVOL 201 sets the water conditions at the inlet section of the HX and the TMDPJUN 202 works instead of the pump, imposing the inlet water Mass Flow Rate (MFR), while the TMDPVOL 205 represents the water outlet.

The expansion tank has been modelled in such a way to accomplish correctly to the function of separator between LBE and argon; on the top of the tank, the TMDPVOL 305 assures the outlet of the gas.

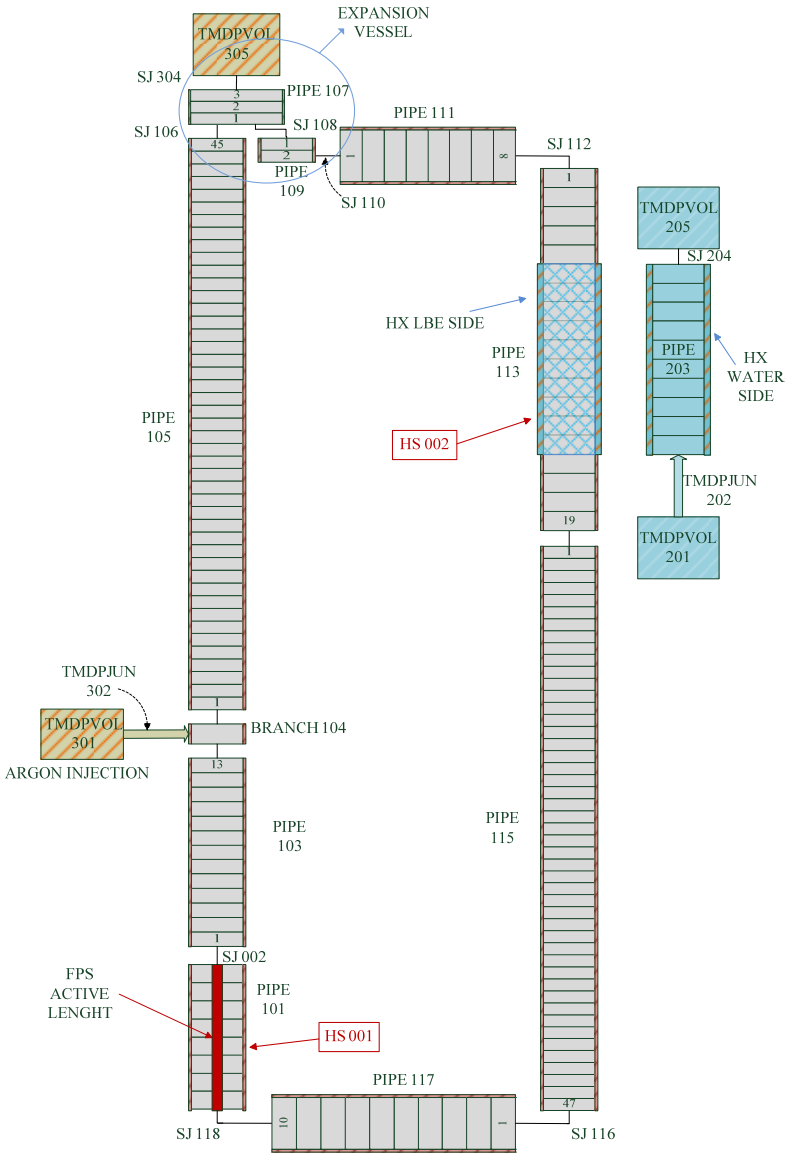

Fig. 4. View of the RELAP5-3D nodalization

Concerning the thermal coupling, the following heat structures (HS) have been introduced:

- HS 001: it reproduces the thermal power supplied by the FPS to the molten LBE;
- HS 002: it simulates the heat exchanged between the primary LBE and the water of the secondary system, simulating the double wall with the steel powder gap;
- Heat structures between the primary loop and the external environment, assuming an insulation of mineral wool with a thickness of 10 cm.

The steel powder thermal conductivity is a function of the temperature and it is affected by different factors, i.e. the grain size and growth, powder density and compaction, thermal cycling. Several experiments have been realized in order to characterize the steel powder from a thermal point of view (Rozzia et al., 2015a) (Rozzia et al., 2015b), with the definition of different sets of experimental correlations.

The thermal conductivity trend, assumed for the R5-3D model, is reported in Fig. 5 and it has been obtained considering an average trend between the "Case A" taken from Rozzia et al., 2015a and "Case B" taken from Rozzia et al., 2015b.

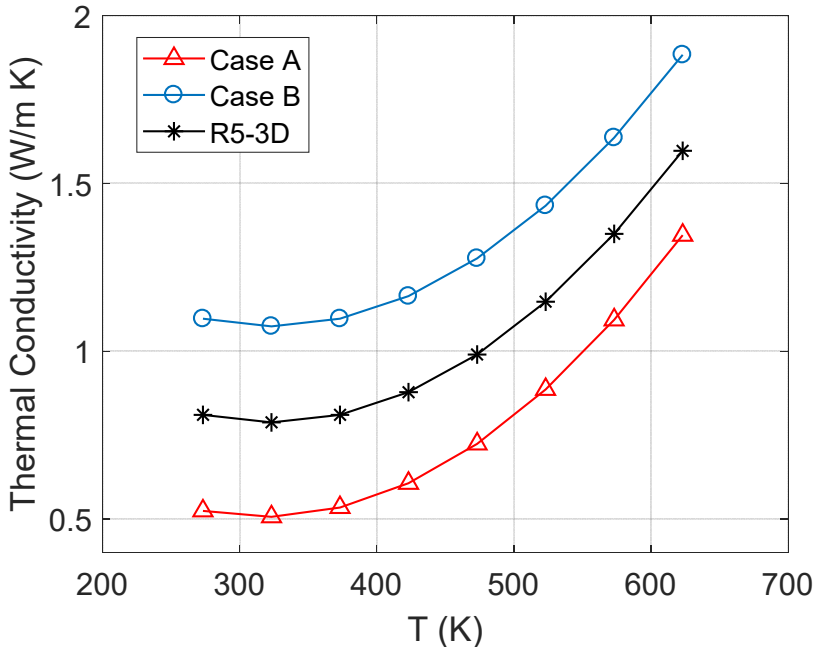

Fig. 5. Stainless Steel Powder Thermal Conductivity

Fig. 6 shows the schematic view of the spacer grid (a) and the upper grid (b). The spacer grid is composed of several stainless-steel rings united each other around the active pins and connected to a bigger central ring. This ring connects itself with the two dummy pins which have a support function. The evaluation of the grids resistance coefficients, dependent on the flow conditions, has been obtained with Rehme correlation (OECD/NEA Nuclear Sceince Commitee, 2015) as follows:

$$K_{grid} = C_v \left(\frac{A_{grid}}{A_{flow}}\right)^2 \tag{1}$$

where A_{grid} is the area occupied by the grid, A_{flow} is the free flow area and C_v is a Reynolds-dependent parameter defined as:

$$C_v = 3.5 + \frac{73.5}{Re^{0.264}} + \frac{2.79*10^{10}}{Re^{2.79}} \tag{2}$$

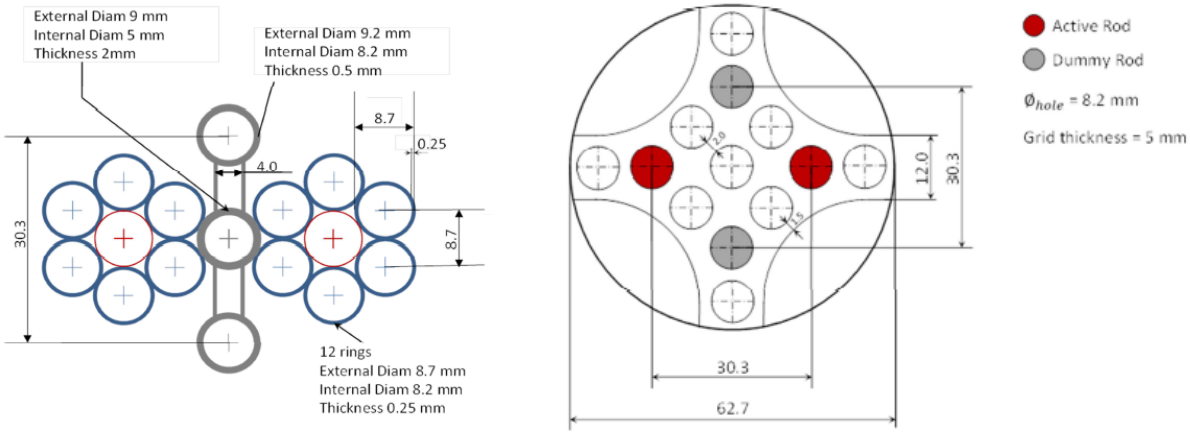

(a) **(b)**

Fig. 6. View of the Spacer Grid (a) and the Upper Grid (b)

An additional singular pressure drop has been introduced to consider the elbow with recess in the lower part of the FPS. The K loss coefficient has been evaluated using the following Reynolds-dependent correlation (Idelchik, 2003):

$$K_{elbow} = 1.2K_{\Delta}K_{Re}C_1AK_{loc} \quad (3)$$

where:

- K_{Δ} and K_{Re} are function of the roughness and Reynolds number respectively;
- C_1 is a geometrical factor (C_1=1 for a circular section);
- A and K_{loc} are geometrical factors.

4. Experimental data vs. RELAP5-3D results

The experimental activity performed on the NACIE facility consists in a series of tests aiming to investigate the system behaviour in conditions of natural circulation (NC), gas-enhanced circulation (GEC) and transition from gas-enhanced to natural circulation (and vice-versa). Of the two electrical pins, only one has been activated on the tests with a maximum power supplied of 22.5 kW. In this work, two tests have been analysed: Test 201 and Test 203, characterized by the boundary conditions reported in Table 4.

The main control parameters are:

- the operating temperature range;
- the percentage of total power supplied by the pins;
- the time ramp to reach the bundle power requested;
- the activation or non-activation of the gas injection device and the secondary side of the heat exchanger.

Table 4. NACIE Test Matrix

Test	$T_{av\ LBE}$ [K]	Power %	Power (kW)	Ramp t (min)	Heat sink	Gas lift (Nl/min)	Transition NC to GEC	Transition GEC to NC
201	473-523	50	9.5	5	YES	0	NO	NO
203	473-523	50	9.5	5	YES	5	NO	YES

In the following, the two experimental tests are presented and discussed, and the results of the numerical simulations are compared with the experimental data. The parameters under investigation are the LBE MFR and the operating temperature range, especially the inlet and outlet temperature of the FPS and the HX, for both primary and secondary loop.

For the experimental estimation of the LBE mass flow rate under steady state condition, for both the natural and gas enhanced circulation tests, the results from the direct measurement of the inductive flow meter (MP101) and from the application of the Energy Balance (EB) equation across the heat source are reported. For the energy balance the relation is:

$$W = \frac{\dot{Q}_{HS}}{c_{p(LBE)}\Delta T_{HS}} \tag{4}$$

where: W is the LBE MFR, $\dot{Q}_{HS}$ is the power generated from the heat sources, c_p is the specific heat of the LBE set to 146.5 J/(kg K), ΔT is the temperature drop across the FPS.

The LBE temperatures at the FPS inlet and outlet section have been measured by the thermocouples (TCs) T109 and T105, the temperatures at the inlet and outlet sections of the HX are measured by TCs T103 and T104, while the inlet and the outlet temperature of the water in the shell side of the HX are measured by the thermocouples T201 and T202.

4.1. Test 201

The aim of this test is the characterization of the LBE flow in case of pure natural circulation regime.

The experimental trends of the power, argon flow rate, water inlet temperature and water MFR have been reproduced and implemented in the R5-3D model as boundary conditions (BC) for a better thermal-hydraulic characterization.

Fig. 7 reports the comparison between the experimental data and numerical results in terms of LBE mass flow rate (Fig. 7 (a)) and temperature in the FPS (Fig. 7 (b)). In Fig. 7 (a) the LBE mass flow rate calculated by R5-3D is compared with the MFR measured by the inductive flow meter MP101 and with the value obtained applying the energy balance (EBMFR). For both Test 201 and Test 203, the reference values for the comparison are those obtained by the energy balance equation, while the MP101 data are not considered because the direct measurements can be affected by error due to the instrument calibration. It can be noticed as the R5-3D value in natural circulation is about 4.0 kg/s, slightly higher than the value deriving from the EB equation.

Fig. 7 (b) compares the temperature trends measured by TCs T109 (FPS inlet) and T105 (FPS outlet), with the LBE temperature calculated at the inlet and outlet section of the heat source. It is possible to notice that the numerical results match in a good way the experimental data, with a smaller LBE ΔT due to the higher mass flow rate.

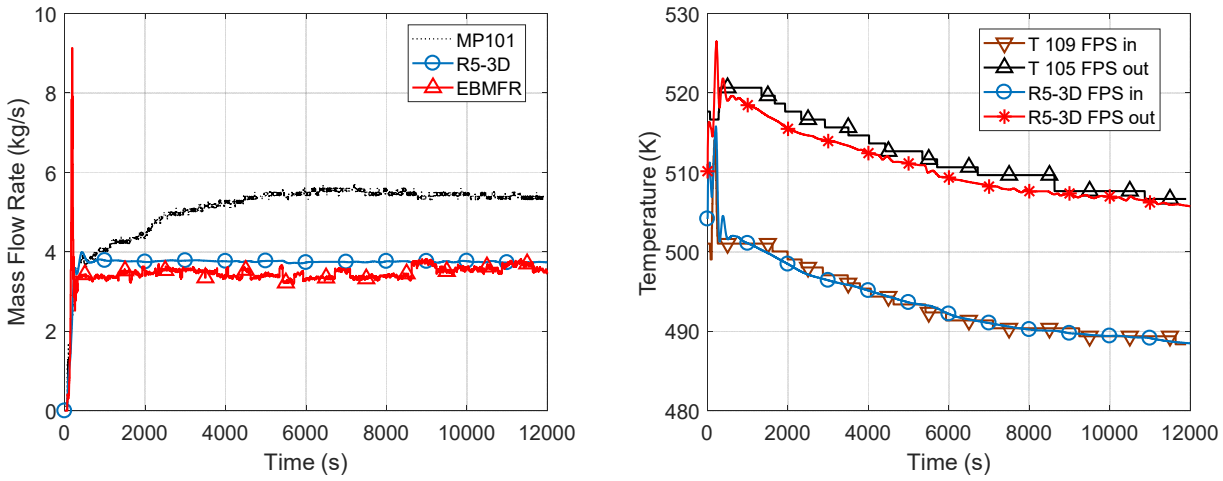

(a) (b)

Fig. 7. TEST 201, LBE mass flow rate (a) and FPS temperatures (b), experimental vs R5-3D

Fig. 8 (a) shows the comparison between the experimental LBE temperature measured by TCs T103 and T104, respectively at the HX inlet and outlet, and the R5-3D LBE temperature. Fig. 8 (b) compares the temperature acquired by TCs T201 and T202 with the water temperature calculated at the inlet and outlet section of the HX secondary side. The temperatures computed by R5-3D are very close to the experimental data: the HX inlet temperature is ~2 K lower than the value measured, with a ΔT inlet-outlet of about 14.5 K, while also for the water temperatures, the trends simulated overlap with a good agreement the experimental ones.

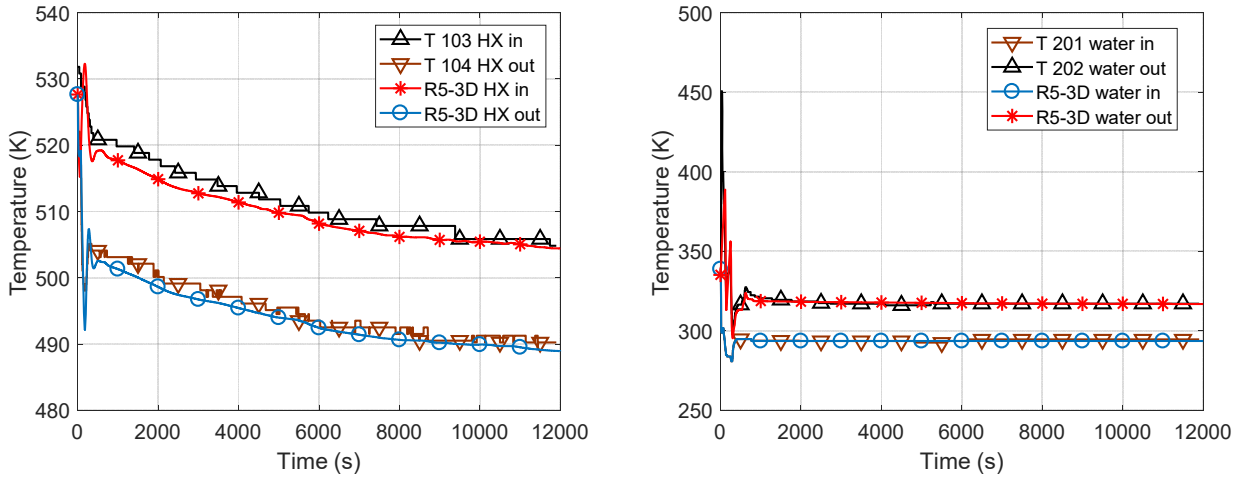

(a) **(b)**

Fig. 8. TEST 201, inlet and outlet temperatures of the LBE (a) and the water (b) in the heat exchanger, experimental vs R5-3D

4.2. Test 203

This test aims to investigate the system behaviour under GEC regime and, afterwards, the transition from GEC to NC regime.

The mass flow rate is shown in Fig. 9 (a) for MP101 flow meter, EB equation and R5-3D. Thanks to the contribution of the argon injection, the mass flow rate in GEC is about 10 kg/s, a value higher than the NC, demonstrating the capability of the gas injection system to sustain the mass flow rate. The code follows with a good agreement the mass flow rate for both GEC and NC, reproducing the

transient trend with good accuracy. Also for the LBE temperatures at the FPS inlet and outlet (see Fig. 9(b)), the comparison with the R5-3D outcomes shows as the values reached during the simulation overlap with a good agreement the measured ones, with a ΔT inlet-outlet of ~6.3 K in GEC and 15.6 K in NC.

Concerning the heat exchanger, Fig. 10 reports the inlet and outlet temperatures on the primary side (a) and secondary side (b), showing a good agreement between the experimental data and the numerical results.

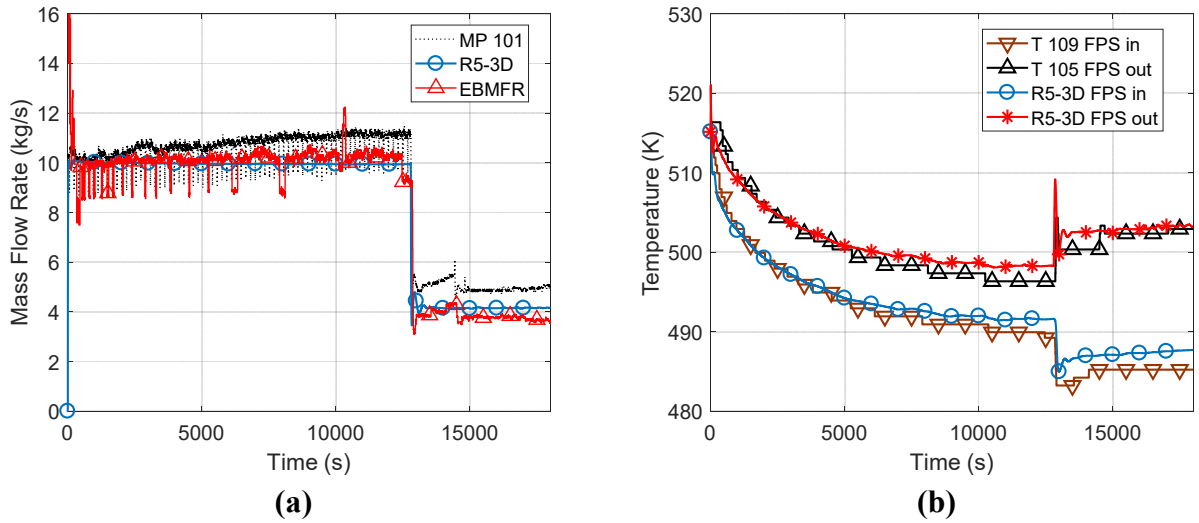

Fig. 9. TEST 203, LBE mass flow rate (a) and FPS temperatures (b), experimental vs RELAP5-3D

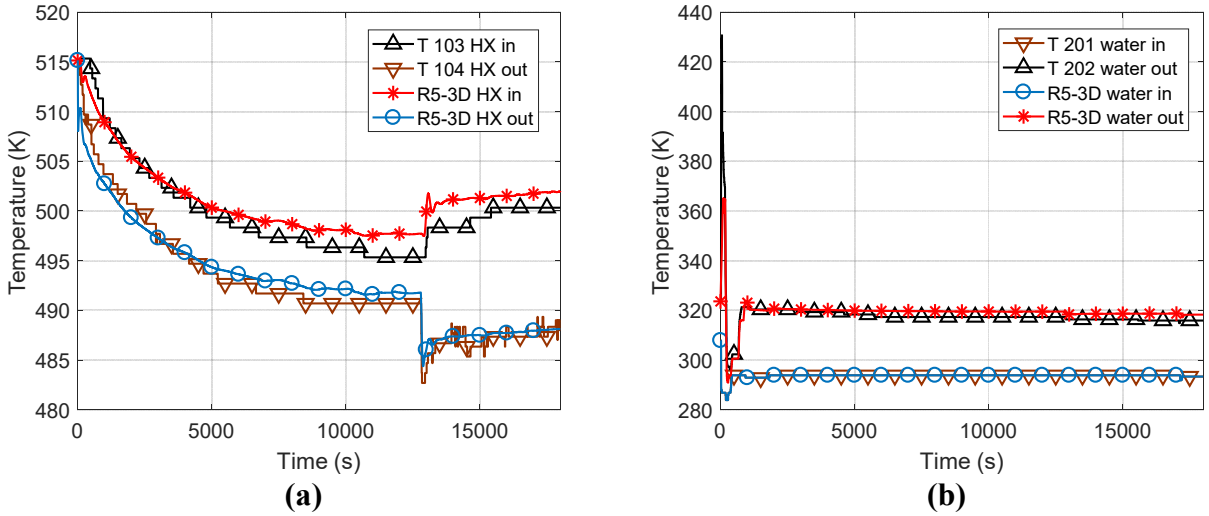

Fig. 10. TEST 203 Temperature at the inlet and outlet section of the primary (a) and secondary (b) circuits

5. Probabilistic comparison metrics

The validation of simulation codes (e.g. RELAP5-3D) is always a fundamental process in the development and assessment of the accuracy of the employed physical models. The state-of-art methodology is well described in Oberkampf et al., 2010. Such approach treats uncertainties individually (i.e. each uncertain parameter is considered distinctly from one another), while the RAVEN proposed methodology path performs the exploration of the input space considering the associated uncertainties altogether and analyzes the responses with several validation metrics.

Uncertainties in the input space are taken into account separately from ones in the output space. Such distinction is performed employing sampling of the input space. Such capability, available in the RAVEN code, permits to compare a larger sample of data (Alfonsi et al., 2017).

In order to assess the accuracy of the physical model under consideration, it is fundamental the inclusion of the experimental data uncertainties. Those uncertainties are going to be directly mirrored in the input space of the experiment, being modeled with the system code under investigation. The uncertainties associated to the input space can be represented by Probability Density Functions (PDFs); when dealing with experiment uncertainties, it is common practice to use the following PDFs, sorted in ascending order of "knowledge" regarding the uncertainty sources:

- Uniform PDF: used when no knowledge of the dispersion and mean of the data are available, but only the variation boundaries (i.e. lower and upper boundaries);
- Triangular PDF: utilized when the variation boundaries and the most probable mean are known, but no information on the dispersion of the data are available;
- Normal PDF: used when information about the mean and dispersion is available.

When the representative uncertainties have been selected, the physical model needs to be perturbed following a sampling strategy. Several sampling strategies are available in the RAVEN code. Traditionally, a Monte Carlo sampling is generally performed since completely independent (in terms of output Figure of Merit (FOM) convergence) on the number of the uncertainties to be propagated (Alfonsi et al., 2014).

Once the uncertainties have been propagated employing a sampling strategy, the final goal of the validation assessment is the comparison of the results (output FOMs) with the experiment measured FOMs (including the associated uncertainties). In the RAVEN code, three main probabilistic comparison metrics are available: CDF (Cumulative Density Function) area metric, PDF area metric and the difference PDF metric (Rabiti et al., 2017). In the following sections, a brief introduction of the three metrics is reported.

The CDF area metric, also called Minkowsky L1 metric, calculates the area difference between the code output CDF_c and the experimental CDF_e using the following equation:

$$d(CDF_c(x), CDF_e(x)) = \int_{-\infty}^{+\infty} \|CDF_c(x) - CDF_e(x)\| \, dx$$

This metric has the same units of the compared FOM x and provides an estimation of the integrated distance between the simulated results and the experiment considering all the propagated uncertainties (see Fig. 11).

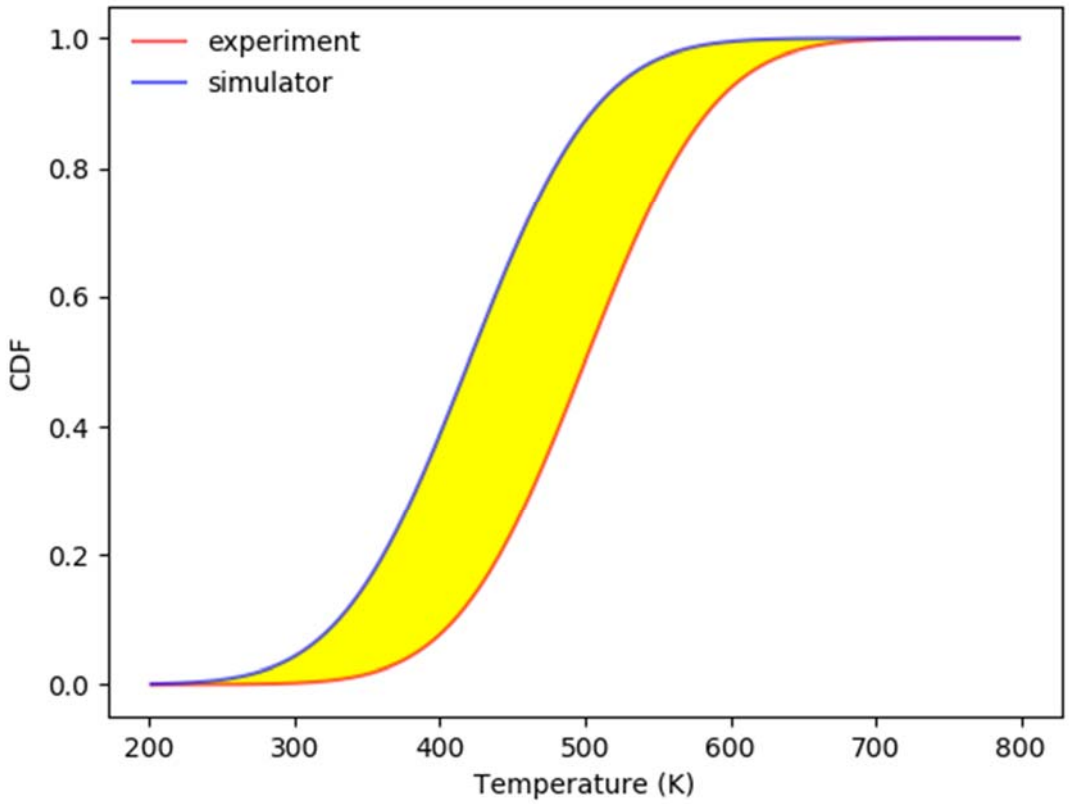

Fig. 11. CDF area metric example

The PDF area metric is aimed to compute the degree of agreement between the PDFs constructed with the experimental and simulated data. It computes the common area between the two PDFs. The resulting computed metric varies between 0.0 (no agreement) to 1.0 (perfect agreement), following the following equation:

$$d_{p.u.}\left(PDF_c(x), PDF_e(x)\right) = \int_{-\infty}^{+\infty} min(PDF_c(x), PDF_e(x))\, dx$$

As graphically shown in Fig. 12, the PDF area is represented by the yellow region.

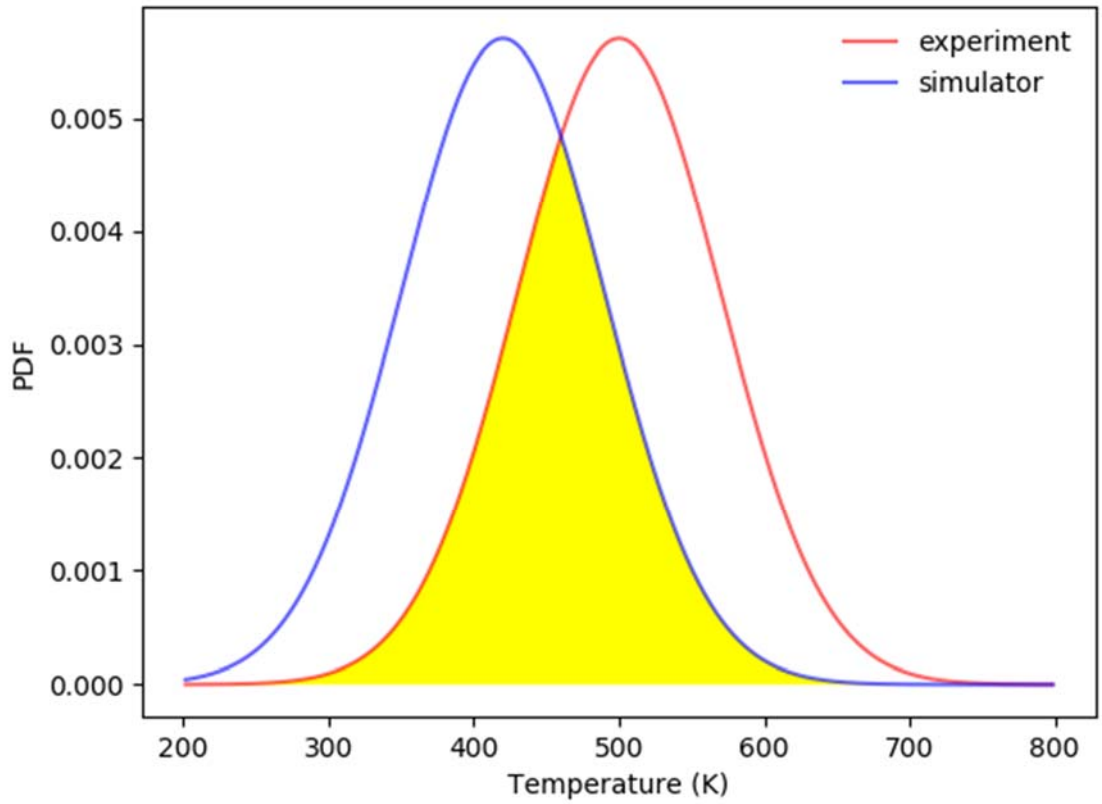

Fig. 12. PDF area metric example

The difference PDF metric is a newly developed, by the RAVEN team, comparison metric. Being z a continuous random variable equal to the difference of two random variables (z = x - y), and being the two random variables statistically independent, the PDF of the difference is computed with the following equation:

$$f_Z(z) = \int_{-\infty}^{+\infty} f_X(x) f_Y(x - z)\ dx$$

This produces a PDF that contains information about the difference between the two PDFs, fX(x) and fY(y). The mean can be calculated as:

$$\bar{z} = \int_{-\infty}^{+\infty} z f_Z(z)\ dz$$

This metric is quite useful for the engineer since it provides a way to define the probability of the signed difference between the experiment and the simulation. For example, Fig. 13 shows the PDF of the distance between an experiment and a simulator response. The integral of the PDF distance metric provides a simple tool to assess the probability of the distance between the experiment and the simulator response. For example, Fig. 14 (red line) shows that the difference between the temperature predicted by the simulator and the experiment has a probability of 25% to be less equal to 75 K.

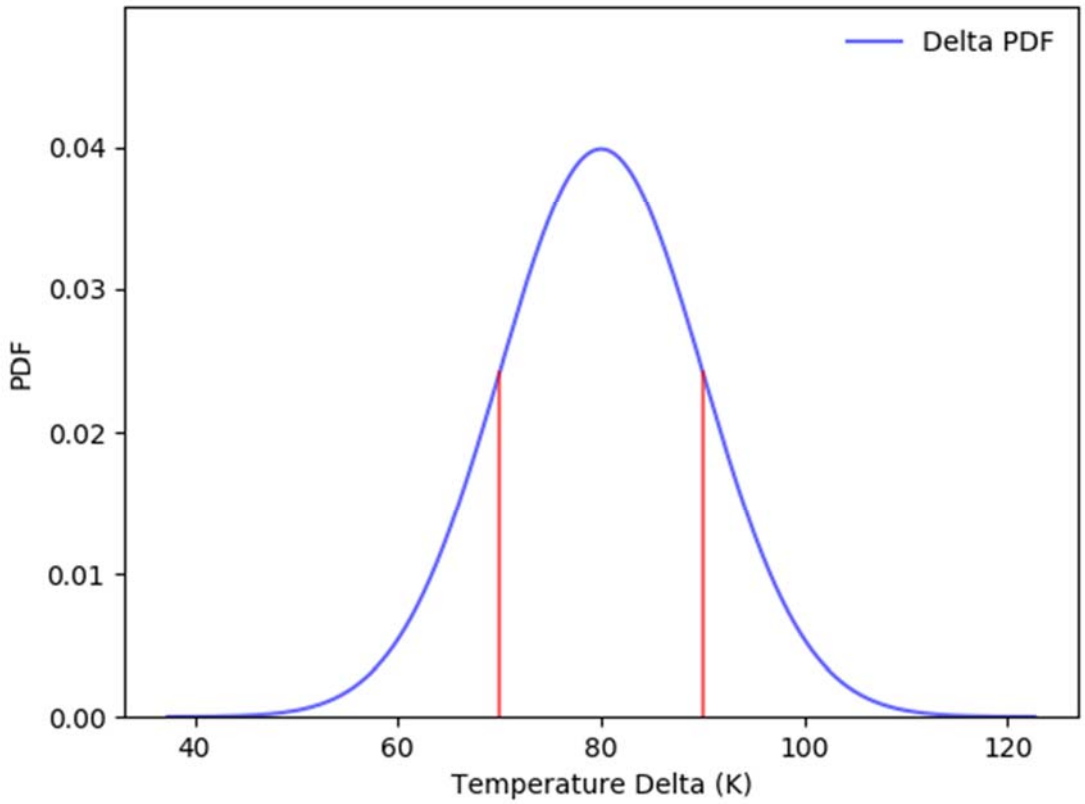

Fig. 13. PDF difference metric example

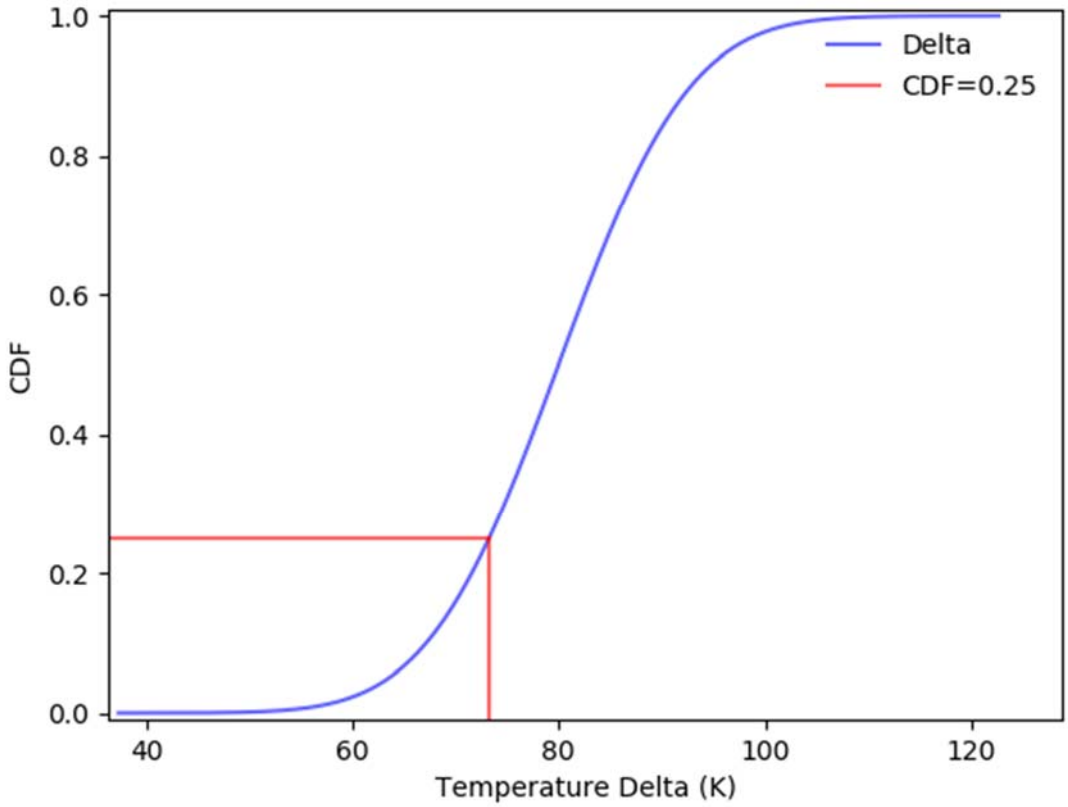

Fig. 14. Integral function (CDF) of PDF difference metric example

6. Raven Calculation

The first step of a statistical strategy is the identification of the parameters which mainly influence the response of the system. The parameters are divided into two set: the independent and the dependent parameters. The first ones are the quantity set up in the experiment and they represent the initial and boundary conditions of the simulation; the second ones are the FOM that consists of the most representative variables monitored during the experiment which will be the objects of the comparison with the system code results. The studied cases consist of a NC and a transition from GEC to NC experiments; the main independent variables are the initial temperature (primary and secondary side), the power supplied to the facility, the feed-water mass flow rate and the argon injection. In addition, the powder thermal conductivity, influenced by a multitude of factors, is a considerable source of uncertainties and it is added to the set of the independent variables. Except for the powder thermal conductivity, the uncertainties on the input parameters are related to the precision (3σ) of the measurement system. About the powder thermal conductivity, a variability of 10 % has been assumed. The selected uncertainty parameters are summarized in Table 5.

Table 5. Selected uncertainty parameters (3σ)

Test	T_{LBE}	Power	FW mass flow rate	T_{FW}	Argon injection	Powder Conductivity
201	+/- 1.5 K	+/- 3%	+/- 10%	+/- 1.5 K	-	+/- 10%
203	+/- 1.5 K	+/- 3%	+/- 10%	+/- 1.5 K	+/- 0.5%	+/- 10%

According to the Wilks formula (Wilks, 1941), considering the two-sided statistical tolerance interval, 93 samples are required to obtain a maximum response with a 95% confidence level and 95% probability. In order to improve the statistical outputs results and to account for the failure of some calculation, 3000 sample runs with random sampled input are carried out for each test and the selected data are collected to identify the uncertainty band of the most representative results.

Fig. 15 and Fig. 16 show the main results of the calculation comparing the experimental data with the expected value (expval) and the 95% and 5% percentile extrapolated from the RAVEN result database. According with the R5-3D results, shown in the previous section, the expected value well reproduces the experimental trend in each test. The percentile offers an estimation of the uncertainty range of the results; as shown in Fig. 15 (a) and in Fig. 16 (a), the LBE mass flow uncertainty range is rather limited, especially in TEST 201, where the primary mass flow rate only depend of the buoyancy phenomenon. In TEST 203 the transition from GEC to NC is well reproduced and the uncertainty range is larger during the first phase, due to the uncertainty on the gas injection system. Fig. 15 (b) (c) and Fig. 16 (b) (c) highlight the comparison of the FPS and HX inlet and outlet temperature; in each test the expected value well predicts the experimental trend, but the uncertainty range is much higher than the mass flow rate uncertainty. This is due to the powder thermal conductivity which represents the major source of uncertainty and it also affects the uncertainty on the feed-water outlet temperature, shown in Fig. 15 (d) and Fig. 16 (d).

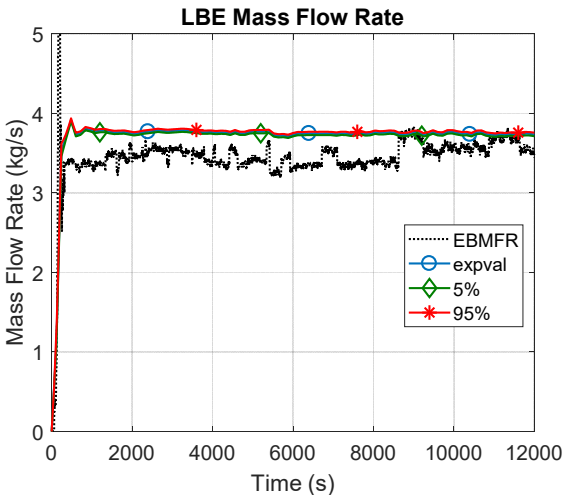

(a)

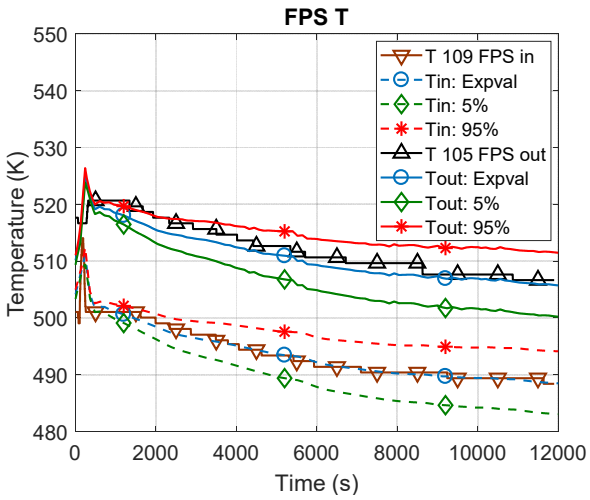

(b)

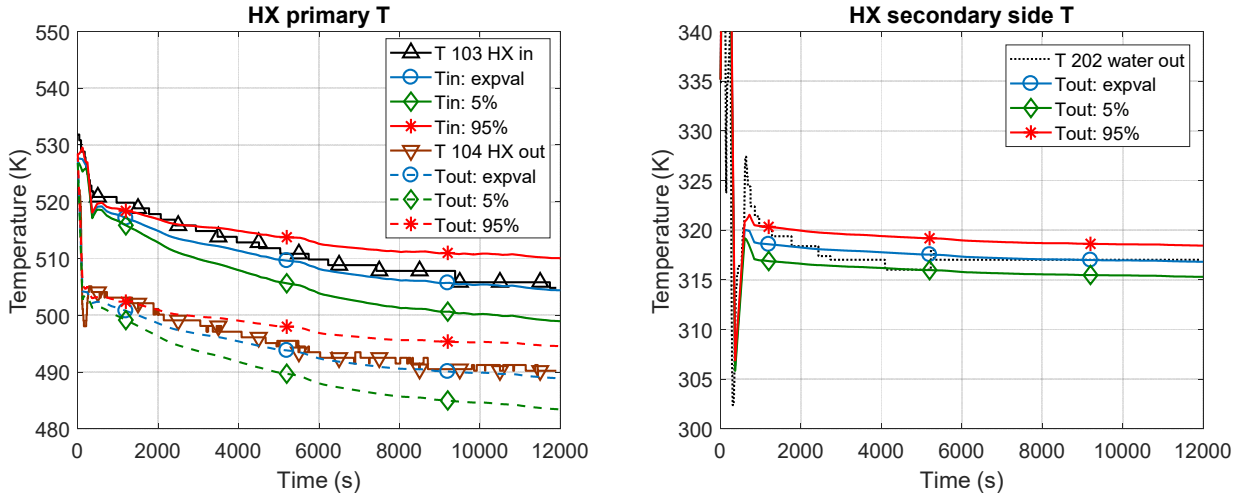

Fig. 15. TEST 201 Main Results

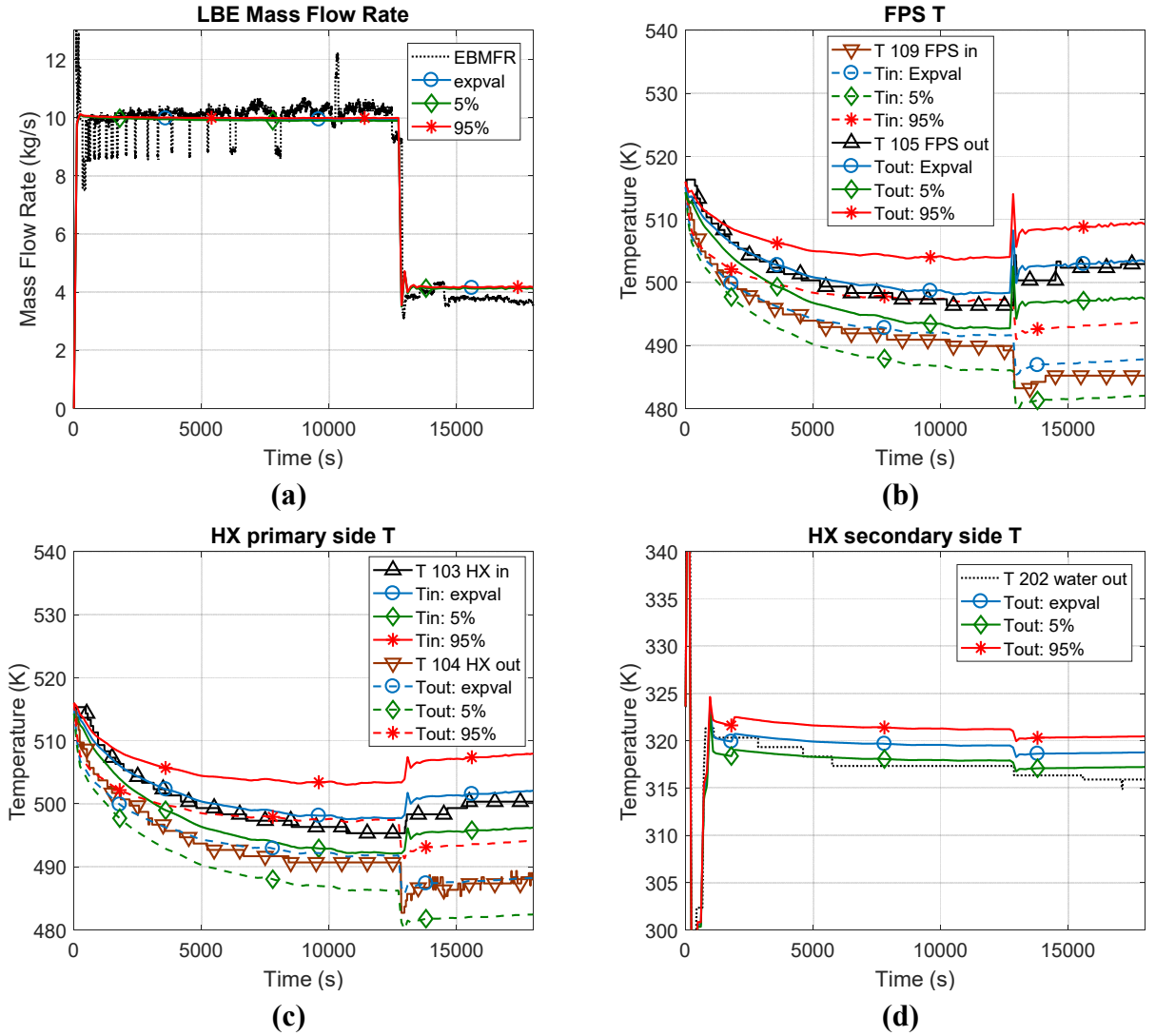

Fig. 16. TEST 203 Main Results

RAVEN uses an automatic binning algorithm to subdivide the output data and minimize the noise caused by the statistical sampling; when all the data collected are divided in the optimized number of

bins, the probabilistic curves are constructed. The number of counts per each bin is normalized to one and summed up bin by bin; a quadratic interpolation is used to fit the data and the CDF curve is obtained. Starting from the cumulative distribution function, the derivative is calculated in order to compute the PDF curve. The computed probabilistic curves are compared with the experimental data, assuming for these a normal distribution, using the measured value as the mean and the precision of the instrumentation as the 3σ (see Table 5). In this section, three examples are analysed to highlight the capability of the methodology.

The computed mean value and variance of each output FOM are summarized in Table 6, where it has been compared with the experimental data and the associated uncertainties. One relevant instant is chosen for the TEST 201 (12000 s, representative of the NC conditions) and two for the TEST 203 (12000 s and 18000 s, representative of the GEC and NC conditions).

As shown in Fig. 15 (a), the LBE mass flow rate computed by R5-3D, in TEST 201, is characterized by a little uncertainty; the comparison between the probabilistic curve of the experimental data and the computed value at the end of the test is shown in Fig. 17. The main outcome is that the model predicts rather well the mean value of the mass flow rate, but it provides a lower value of the standard deviation. Two are the possible reasons: the model is not able to predict the experimental propagation of the uncertainty or some relevant uncertainties of the system have been omitted in the model. In this case, and also in the LBE mass flow rate of TEST 203 (see Table 6), the second thesis seems right. As shown in Fig. 7 (a), the MFR measured by the flow meter is affected by error due to the calibration of the instrument and the mass flow obtained with the energy balance equation is used for the comparison. This value is characterized by uncertainties due to the measurement of the temperatures and also by uncertainties related to the specific heat in the balance equation which is not included in the model.

Fig. 18 shows the comparison of the LBE temperature at the inlet section of the FPS. The code well reproduces the mean value, but it predicts a larger standard deviation than the experimental data. In this case, or the model is not able to attenuate the propagation of the uncertainties or the uncertainties on the input data has been not well estimated. As shown in Fig. 5, the stainless-steel powder thermal conductivity represents a high source of uncertainty, due to the lack of information. This causes the high value of the standard deviation of all LBE temperatures, larger than the standard deviation associated to the precision of the thermocouples; so, the second thesis seem to be right.

For the TEST 203, Fig. 9 and Fig. 10 show a good agreement between the computed outcomes and the experimental data. The LBE mass flow rate is well predicted by the code during the GEC phase but it is slightly overestimated after the transition to NC conditions. Fig. 19 shows the comparison of the primary MFR in NC. An error on the mean value is added to the underestimation of the standard deviation already analysed in Fig. 17; the model could not predict very well the transition from the GEC to the NC conditions or a wrong measurement of the mass flow could be occurred. In this case, the analytical methodology for the measurement of the MFR could explain the inconsistency between the computed results and the experimental data.

Table 6. Probabilistic Analysis: main results

			Experimental data		**Simulation results**	
	FOM		Mean	σ^2	Mean	σ^2
Test 201	**LBE Mass flow rate**	kg/s	3.7	3.50E-03	3.7	1.70E-04
	FPS inlet T	K	488.6	0.25	488.5	11.43
	FPS outlet T	K	506.7	0.25	505.7	11.85

	HX inlet T	K	504.8	0.25	504.4	11.49
	HX outlet T	K	490.2	0.25	488.9	11.56
	LBE Mass flow rate	kg/s	10.2	2.66E-02	9.9	8.16E-04
Test 203 GEC	**FPS inlet T**	K	489.9	0.25	491.8	11.30
	FPS outlet T	K	496.3	0.25	498.4	11.39
	HX inlet T	K	495.3	0.25	497.8	11.26
	HX outlet T	K	490.7	0.25	491.9	11.34
	LBE Mass flow rate	kg/s	3.65	3.50E-03	4.15	2.21E-04
Test 203 NC	**FPS inlet T**	K	485.2	0.25	487.8	12.41
	FPS outlet T	K	502.9	0.25	503.3	12.80
	HX inlet T	K	500.3	0.25	502.1	12.55
	HX outlet T	K	488.4	0.25	488.2	12.49

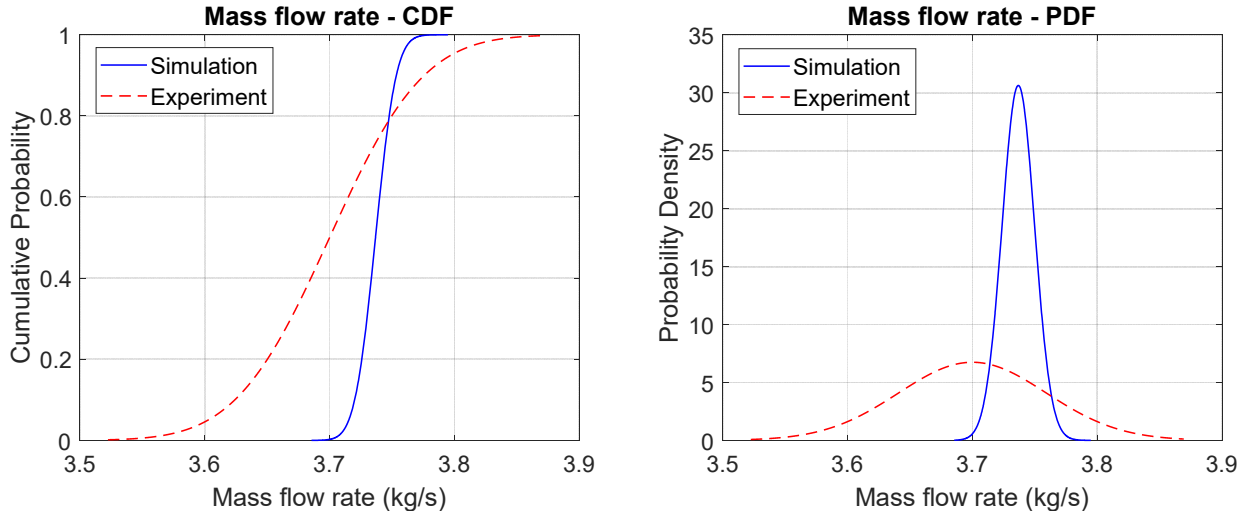

(a) **(b)**

Fig. 17. TEST 201 (12000 s): LBE mass flow rate

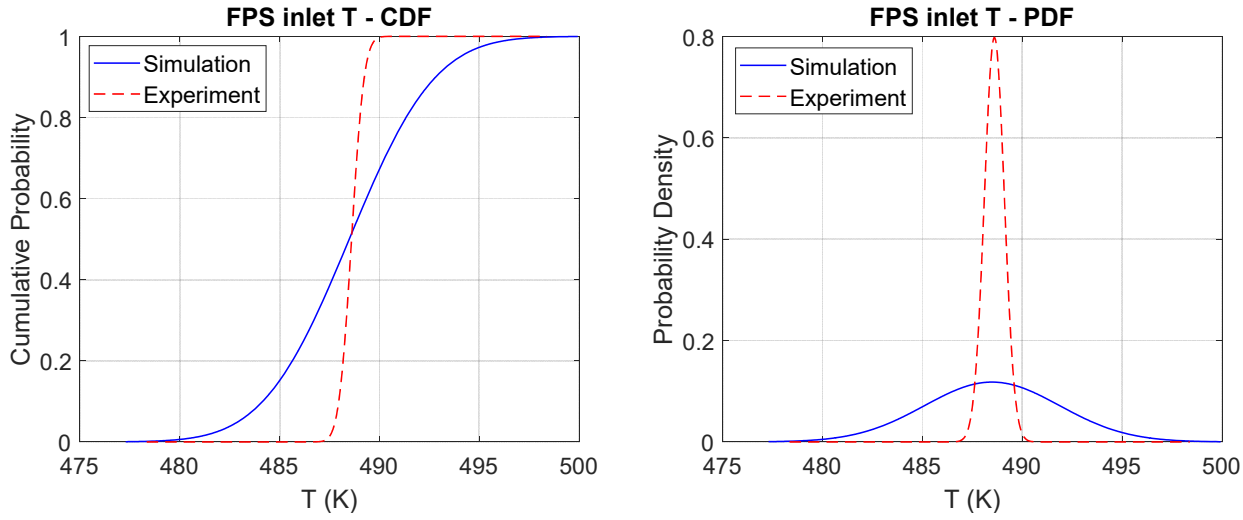

(a) **(b)**

Fig. 18. TEST 201 (12000 s): FPS inlet temperature

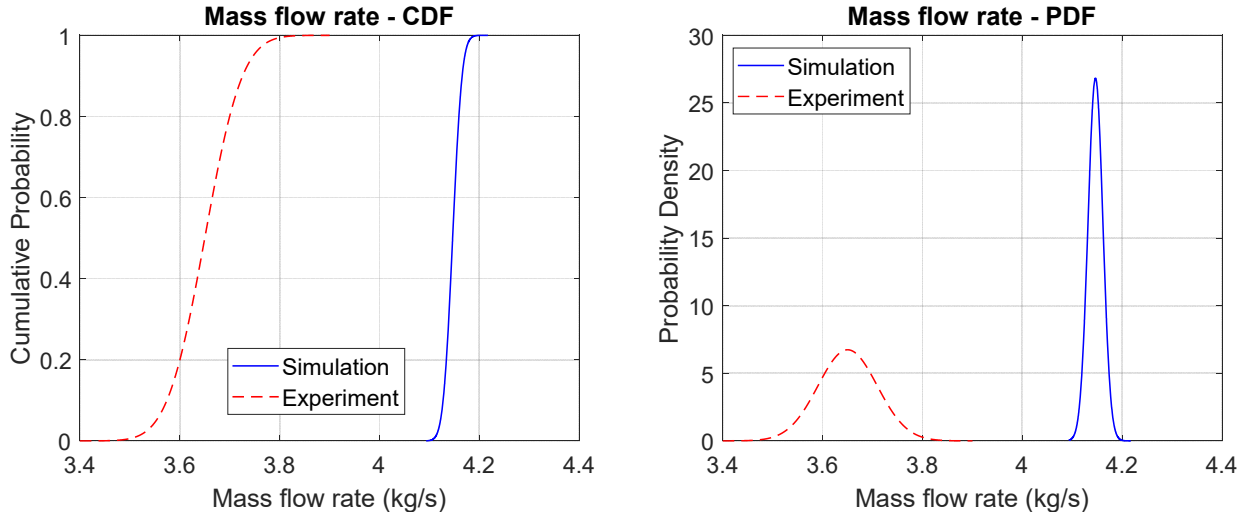

Fig. 19. TEST 203 (18000 s): LBE mass flow rate

Fig. 18 (a) shows a good prediction of the mean value of the LBE temperature at the FPS inlet; if the analysis of the calculation outcomes was founded only on the mean value, we would not obtain perfect information about the discrepancy between the simulated results and the experimental data. The CDF area metric provides this information in the same units of the compared FOM. Table 7 summarizes the outcomes of this metric; about the LBE temperature, the average difference between the CDFc and the CDFe is 2.5 K. The maximum value is obtained for the HX outlet temperature, where the difference is about 3 K. A good agreement is observed for the LBE mass flow rate, where the CDF area difference is lower than 0.5 kg/s in all three cases. Even if, as shown in Fig. 19 (a) the mean value of the primary mass flow in natural circulation conditions (TEST 203) is not well predicted, the difference between the simulated outcomes and the experimental data is always below 0.5 k/s.

The PDF area metric provides a bit different results than the previous metric. This analysis computes the degree of agreement between the PDF curves but it losses information about how far apart the two set of data are. This is the case of the LBE mass flow rate in NC during TEST 203; Fig. 19 (b) shows that the common area between the PDFs is essentially zero (see also Table 8) but the previous metric highlights that the discrepancy between the calculated value and the experimental data is lower than 0.5 kg/s, highlighting a good prediction of R5-3D.

The last one is the difference PDF metric which provides several useful information. Fig. 20 (b) shows the PDF of the difference between the two probability density functions depicted in Fig. 17 (b). The mean of this PDF provides an information about the mean value of the difference between the experimental data and the simulated outcome; the more the mean values are close, the more the mean of this PDF is close to zero. Fig. 20 (b) shows that the mean difference is -0.028 kg/s and the uncertainty is contained between -0.3 and 0.25 kg/s. The CDF of the difference is obtained integrating the PDF. This curve offers useful information to the engineers; it is able to provide the probability to obtain a difference below a certain value. For example, Fig. 20 (a) shows the CDF of the difference for the LBE mass flow rate in TEST 201. The probability to obtain a discrepancy between the computed value and the experimental data below 0.0 (i.e. between -0.3 and 0.0 kg/s) is 70 %. In the same way, the probability to obtain a difference between -0.3 and -0.1 is 10%. This metric provides useful outcomes on the definition of the safety margins for the NPP design.

Fig. 22 shows the PDF and the CDF of the difference for the LBE mass flow rate in natural circulation conditions (TEST 203). The PDF area metric highlights the no matches between calculated and experimental values; the difference PDF metric shows the same results (the difference is always negative both in PDF and CDF curve) but it provides additional information on the probability to obtain specific difference between the simulation and the experiment.

Table 7. CDF Area Difference

CDF Area Difference

Test (Condition)	LBE Mass Flow Rate (kg/s)	FPS inlet T (K)	FPS outlet T (K)	HX inlet T (K)	HX outlet T (K)
201 (NC)	0.045	2.49	2.86	2.59	2.99
203 (GEC)	0.274	2.44	2.51	2.64	2.36
203 (NC)	0.492	2.78	2.59	2.56	2.70

Table 8. PDF Common Area

PDF Common Area

Test (Condition)	LBE Mass Flow Rate	FPS inlet T	FPS outlet T	HX inlet T	HX outlet T
201 (NC)	35.85%	24.13%	20.65%	23.12%	19.51%
203 (GEC)	9.13%	26.85%	27.07%	27.31%	25.87%
203 (NC)	1.8E-12%	26.24%	22.81%	26.05%	21.56%

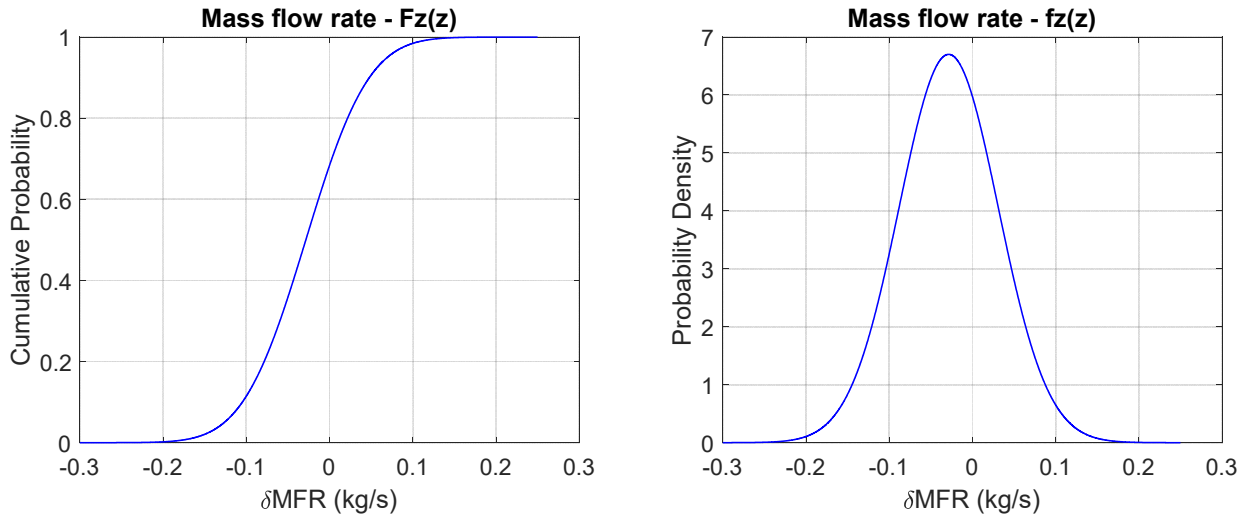

(a) **(b)**

Fig. 20. Difference PDF metric: TEST 201 LBE mass flow rate (12000 s)

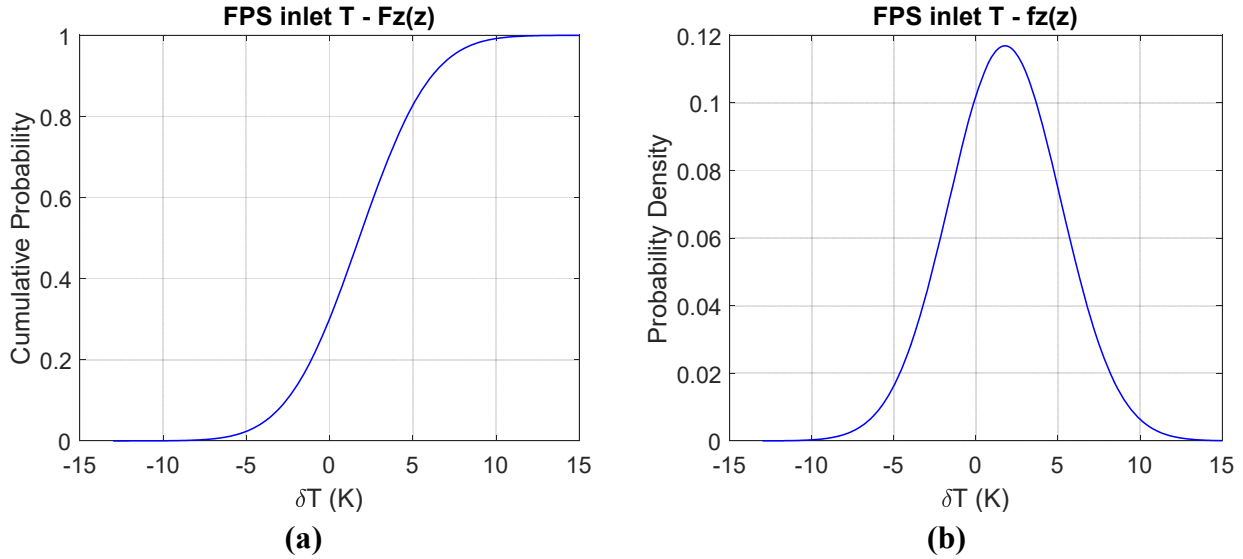

(a) **(b)**

Fig. 21. Difference PDF metric: TEST 201 FPS inlet temperature (12000 s)

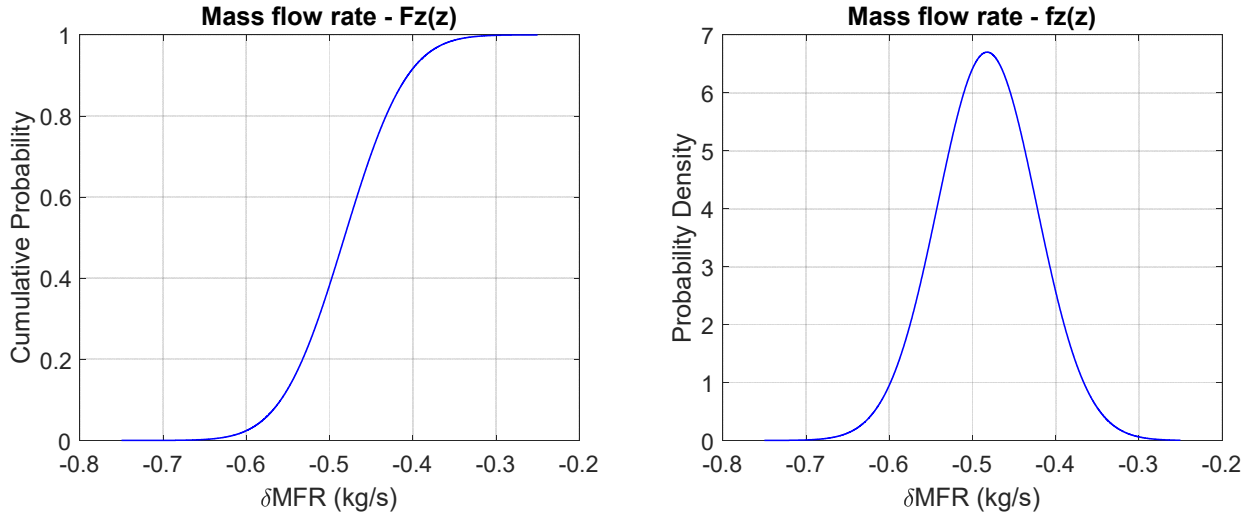

(a) **(b)**

Fig. 22. Difference PDF metric: TEST 203 LBE mass flow rate (18000 s)

7. Conclusions

The objective of the activity has been to verify a coupled RELAP5-3D©/RAVEN methodology for the uncertainty quantification on HLM system. At this purpose, a mono-dimensional model for NACIE facility has been developed and the post-test calculations have been carried out using RELAP5-3D© ver. 4.3.4. Two experimental tests have been selected for the activity: the TEST 201 which aimed to investigate thermal-hydraulics on pure natural circulation conditions regime, and TEST 203 that aimed to analyse the system behaviour in the transition between GEC and NC regime. The post-test calculation has verified the capability of the model to predicts the main experimental outcomes, but this is not sufficient to perform a safety analysis. In this framework, the BEPU method plays a key role in the development of innovative GEN-IV reactors. At this purpose, the activity aims to verify a BEPU methodology based on the RAVEN code, developed at Idaho National Laboratories.

Starting from the post-test results, the independent parameters space has been perturbed following a Monte Carlo sampling. The uncertainties have been propagated and the main results are collected

in a database. The final step has been the comparison of the calculated FOMs and the experimental measured results, including the associated uncertainties. Three comparison metrics, fully integrated in RAVEN, have been adopted and the main results have been analysed. According to the post-test calculations, the comparison metrics has shown good results in terms of mean values, but they also have highlighted a not optimal uncertainty prediction due to the lack of some input information, especially related to the stainless-steel powder thermal conductivity.

This work has highlighted the capability of the BEPU method; the methodology will be applied to a more complex system which reproduces the primary system of a LFR (Narcisi et al., 2017) and to an innovative steam generator developed for the ALFRED reactor (Narcisi et al., 2018).

List of Acronyms

BC	Boundary Condition
BEPU	Best Estimate Plus Uncertainty
CDF	Cumulative Density Function
EXPVAL	Expected Value
FOM	Figure of Merit
FPS	Fuel Pin Simulator
GEC	Gas-enhanced Circulation
GEN-IV	Generation IV
GIF	Generation IV International Forum
HLM	Heavy Liquid Metals
HS	Heat Structure
HX	Heat Exchanger
LBE	Lead-Bismuth Eutectic
LFR	Lead-cooled Fast Reactor
LWR	Light Water Reactor
MFR	Mass Flow Rate
NACIE	NAtural CIrculation Experiment
NC	Natural Circulation
NPP	Nuclear Power Plant
PDF	Probability Density Function
R5-3D	RELAP5-3D© ver. 4.3.4
R&D	Research and Development
STH	System Thermal-Hydraulic
EB	Energy Balance
EBMFR	Energy Balance Mass Flow Rate
TC	Thermocouples
UQ	Uncertainty Quantification

Acknowledgements

The authors wish to thank all the ENEA FSN-ING and in particular M. Tarantino and I. DI Piazza for providing NACIE experimental data.

References

Alfonsi, A., Rabiti, C., Mandelli, D., Cogliati, J., Wang, C., Talbot, P. W., Maljovec, D. P., Smith, C., 2017. RAVEN Theory Manual and User Guide. INL/EXT-16-38178

Alfonsi, A., Rabiti, C., Mandelli, D., Cogliati, J., Kinoshita, R., Naviglio, A., 2014. RAVEN and Dynamic Probabilistic Risk Assessment: Software Overview. Eu. Saf. and Rel. Conf., Wroclaw, Poland.

Balestra, P., Giannetti, F., Caruso, G., Alfonsi, A., 2016. New RELAP5-3D lead and LBE thermophysical properties implementation for safety analysis of Gen IV reactors. Sci. Technol. Nucl. Install. 2016. https://doi.org/10.1155/2016/1687946

Coccoluto, G., Gaggini, P., Labanti, V., Tarantino, M., Ambrosini, W., Forgione, N., Napoli, A., Oriolo, F., 2011. Heavy liquid metal natural circulation in a one-dimensional loop. Nucl. Eng. Des. 241, 1301-1309, 10.1016/j.nucengdes.2010.06.048

D'Auria F., Camargo C., Mazzantini O., 2012. The Best Estimate Plus Uncertainty (BEPU) approach in licensing of current nuclear reactors, Nucl. Eng. Des. 248, 317-328, https://doi.org/10.1016/j.nucengdes.2012.04.002

Idelchik, I.E., 2003. Handbook of Hydraulic Resistance, Jaico Pub. House, 3rd ed.

Narcisi, V., Giannetti, F., Tarantino, M., Martelli, D., Caruso, G., 2017. Pool temperature stratification analysis in CIRCE-ICE facility with RELAP5-3D© model and comparison with experimental tests. J. Phys. Conf. Ser. 923 (012006). http://dx.doi.org/10.1088/1742-6596/923/1/012006.

Narcisi, V., Giannetti, Del Nevo, A., Tarantino, M., Caruso, G., 2018. Pre-test analysis of accidental transients for ALFRED SGBT mock-up characterization. Nucl. Eng. Des. 333 181-195, https://doi.org/10.1016/j.nucengdes.2018.04.015

Oberkampf, W. L., Roy, C. J., 2010. Verification and Validation in Scientific Computing, Cambridge University Press., 2nd ed.

OECD/NEA Nuclear Science Committee, 2015. Handbook on Lead-bismuth Eutectic Alloy and Lead Properties, Materials Compatibility, Thermal- hydraulics and Technologies. OECD 2015 NEA. No. 7268 https://www.oecd-nea.org/science/pubs/2015/7268-lead-bismuth-2015.pdf

Queral C., Montero-Mayorga J., Gonzalez-Cadelo J., Jimenez G., 2015. AP1000® Large-Break LOCA BEPU analysis with TRACE code, Annals of Nuclear Energy, 85, 576-589, https://doi.org/10.1016/j.anucene.2015.06.011.

Rabiti, C., Alfonsi, A., Cogliati, J., Mandelli, D., Kinoshita, R., Sen, S., Wang, C., Chen, J., 2017. RAVEN User Manual. INL/EXT-15-34123

Rozzia, D., Fasano, G., Di Piazza, I., Tarantino, M., 2015a. Experimental investigation on powder conductivity for the application to double wall heat exchanger (NACIE-UP). Nucl. Eng. Des. 283, 100–113. https://doi.org/10.1016/j.nucengdes.2014.06.037

Rozzia, D., Forgione, N., Fasano, G., Tarantino, M., Del Nevo, A., Alemberti, A., 2015b. Experimental investigation on powder conductivity for the application to double wall heat exchanger

(NACIE-UP), in: 24th International Conference Nuclear Energy for New Europe. Portoroz, Slovenia, pp. 1–9

Shin, Y. H., Hwang II S., Polidori, M., Meloni, P., Casamassima, V., Cornet, S., Barucca, L., Balestri, D., Jin, M., Viellieber, M., 2014. Cross-Comparison of One-Dimensional Thermal-Hydraulic Codes on Natural Circulation Analysis of NACIE Loop Test for Lead-Alloy Cooled Advanced Nuclear Energy System (LACANES), in in: Proceedings of the 22nd International Conference on Nuclear Engineering, Prague, Czech Republic, doi:10.1115/ICONE22-30716

Tarantino, M., Bernardi, D., Coccoluto, G., Gaggini, P., Labanti, V., Forgione, N., Napoli, A., 2010. Natural and Gas Enhanced Circulation Tests in the NACIE Heavy Liquid Metal Loop, in: Proceedings of the 18th International Conference on Nuclear Engineering. Xi'an, China, pp. 1–10. https://doi.org/10.1115/ICONE18-29968

The RELAP5-3D© Code Development Team, 2015. RELAP5-3D Code Manual Vol.1 Code Structure, System Models and Solution Methods INL/MIS-15

Wilks, S.S., 1941. Determination of Sample Sizes for Setting Tolerance Limits. Ann. Math. Stat. 12, 91–96. https://doi.org/10.1214/aoms/1177731788